EPOXI MRI Photometry of Comet 103P/Hartley 2

06 December 2012

Stephanie McLaughlin, University of Maryland
Jade Williams, University of Maryland
Jian-Yang Li, Planetary Science Institute
Dennis Bodewits, University of Maryland

1 Overview

We perform photometric measurements of comet 103P/Hartley 2 using images taken through the Clear1 (broadband, 200-1100 nm), CN (387 nm), OH (309 nm), C2 (514 nm), and two dust continuum filters (Violet at 345 and Green at 526 nm) of the Medium Resolution Instrument (MRI) on board the Deep Impact flyby spacecraft from 1 October to 26 November 2010 during the EPOXI mission. Our analysis includes over 30,000 MRI science images where the nucleus was not resolved. We apply two different methods for our analysis: simple aperture photometry using circular apertures and azimuthal averaged photometry using concentric annuli to remove stars. The resulting photometry and computed errors from each method are provided as separate flat ASCII tables along with PDS labels describing the layouts and columns. Bodewits, et al. (2013), used these data to help characterize the gas and dust in the coma around Hartley 2.

2 Instrument

The Medium Resolution Instrument consists of a Cassegrain telescope with a 12 cm aperture and a 2.1 m focal length and a CCD. The detector is a 1024x1024 split-frame, frame-transfer CCD with 21-micron-square pixels. The electronics allow readout of centered sub-frames in multiples of 2: 64x64, 128x128, and so on. The net pixel scale is 10 microradians/pixel (2.06265 arcseconds/pixel). MRI images are never binned. The full-width half-max (FWHM) of the point spread function is approximately 1.6 pixels (Klaasen, et al., 2013).

The MRI has nine filters. Some were only used during close-encounter, and our sample only includes these six:

Filter #	Filter Name	Center Wavelength (nm)	FWHM (nm)	Eff. Wavelength (nm)	Comments
1	CLEAR1	650	>700	626.1	Not band limited
2	C2	514	11.8	515.3	For C_2 coma studies
3	GREEN_CONT	526	5.6	526.0	For dust in coma
7	CN	387	6.2	388.8	For coma studies
8	VIOLET_CONT	345	6.8	345.5	For dust in coma
9	OH	309	6.2	309.5	For coma studies

Center wavelength and FWHM values are reported by Hampton, et al., (2005), and effective wavelengths for calibration purposes by Klaasen, et al., (2013).

The physical size of the two central rows of the CCD is 1/6th-pixel shorter in the vertical direction than all other rows (Klaasen, et al., 2013; Klaasen, et al., 2008; Hampton et al., 2005). However, the pipeline reconstructs raw and calibrated images with uniform row spacing, which introduces a 1/3rd-pixel, horizontal extension at the center of the array. Therefore, the actual angular separation of two features on either side of the horizontal midpoint line but outside of the two central rows is 1/3rd -pixel less than the separation measured in a reconstructed image. As for all geometric distortions, the correction for this distortion requires resampling of the image and an attendant loss in spatial resolution. The pipeline does not perform this geometric correction in order to preserve the best spatial resolution. However, it does correct for the 1/6 decrease of signal in the two narrower central rows due to smaller collecting area by the flat-field division so that the pixels in those two rows have the correct scene radiance in the calibrated images. This preserves the surface brightness measurement everywhere in the geometrically distorted image. Point source or disk integrated photometric measurements using aperture photometry that includes these two central rows will be slightly distorted unless special adjustments are made. For example, Appendix A of Belton, et al. (2011), describes the method of subtracting 1/6th-pixel worth of signal from the two central rows and adjusting for the geometric distortion in calibrated MRI images of comet 9P/Tempel 1 before performing photometry. We apply a different approach for Hartley 2 photometry, which is described below. We refer to this process of recovering the original scene radiance as the "gap correction".

3 Summary of Observations

MRI acquired over 41,000 images of the comet during the encounter phase, which began on 05 September 2010. Clear1 and CN filter images were taken frequently throughout this phase. OH, C2, and dust continuum frames were acquired less frequently and only for several days spanning closest approach, which occurred 2010-11-04T13:59:47.31 UTC at a distance of 694 kilometers. The following table summarizes the MRI observations and the cadence of filter imaging throughout the encounter. We note that data acquired on 2010-10-06 were never downlinked due to a pointing problem with the Deep Space Network.

Start & Stop Mid-Obs Dates	**Mission Activity (E = Encounter at closest approach)**
2010-09-05/248 to 2010-09-15/258	Approach imaging E-60 to E-50 days: • Rotation sampling every 6 hours using Clear1 and CN filters
2010-09-15/258 to 2010-09-25/269	Approach imaging E-50 to E-40 days: • Rotation sampling every 2 hours using Clear1 and CN filters
2010-10-01/274 to 2010-10-27/300	Approach imaging E-34 to E-8 days: • Clear1 rotation sampling every 5 minutes • Single CN frame approximately every hour
2010-10-27/300 to 2010-11-03/307	Approach imaging E-8 days to E-18 hours: • Continuous Clear1 rotation sampling, approximately twice per minute, for 16 hours then once every hour

	• 5 CN, 4 OH, and 2 dust continuum frames daily
2010-11-03/307 to 2010-11-04/308	Flyby imaging E-18 to E-3 hours: • Clear1 rotation sampling every 30 minutes • CN, OH, and C2 frames every hour plus occasional dust continuum (Green and Violet) frames
2010-11-04/308 to 2010-11-04/308	Flyby imaging E-2 to E+1.5 hours: • Clear1 imaging every 15 minutes to nearly continuous at closest approach • CH, OH, C2, and dust continuum imaging
2010-11-04/308 to 2010-11-06/310	Flyby imaging E+2 hours to E+2 days: • Clear1 rotation sampling every 30 minutes • CN, OH, and C2 frames every hour plus occasional dust continuum (Green and Violet) frames
2010-11-06/310 to 2010-11-16/320	Departure imaging E+2 to E+12 days: • Continuous Clear1 rotation sampling, approximately twice per minute • 5 CN and OH frames daily
2010-11-16/320 to 2010-11-26/330	Departure imaging E+12 to E+21 days: • Clear1 rotation sampling every 30 minutes • 5 CN frames daily

We exclude two specific subsets of data from our analysis:

- Images acquired within about +/- 5 hours of closest approach because the nucleus was resolved, and
- Images taken from 5 through 25 September (E-60 to E-40 days) because a small light leak at large solar elongations allowed sunlight to enter the instrument, causing the comet to appear anomalously bright in all filters. See the technical report by Bodewits, et al., (2011), included in the documentation for this archive.

4 Photometry Process

Our photometry process consists of the following steps, which we describe below:

1. Start with reversibly calibrated images and a list of comet centroid coordinates as the inputs
2. Assign a quality flag to each image
3. Remove cosmic rays
4. Apply a "gap" correction
5. Perform simple aperture photometry
6. Perform azimuthal averaged photometry
7. Compute photometric uncertainties

4.1 Input Data

4.1.1 Reversibly Calibrated Images

We use the reversibly calibrated (RADREV) MRI science images of Hartley 2 archived in the NASA Planetary Data System (McLaughlin, et al., 2012) as input to this photometric analysis. We restrict data to "good" images taken through the Clear1, CN,

C2, OH, Green Continuum, and Violet Continuum filters where the nucleus was not resolved or contaminated by the anomalous light leak. "Good" images are defined in section 4.2.

The RADREV images have had the standard EPOXI pipeline corrections applied to them: bias and dark frame subtraction, flat-field corrections, horizontal stripe removal (only a minority of CLEAR1), etc. They have not, however, been "cleaned" to remove artifacts such as cosmic rays and bad pixels. For more information about the calibration process, see Klaasen, et al. (2013).

We define the following image display orientation and pixel coordinate notation for our analysis. All RADREV images are displayed using the FITS convention where lines increase up and samples increase to the right. Our pixel coordinate notation is zero based with the first coordinate (0,0) located at the center of the pixel in the lower left corner of the display window, and the pixel coordinate of the center of the a full-frame, 1024x1024 image is (511.5, 511.5). Figure 1 (Klaasen, et al., 2008) shows a full frame MRI image from the Deep Impact prime mission displayed with this convention. We refer to quadrants A and B as the top or upper half of the image and quadrants C and D as the bottom or lower half.

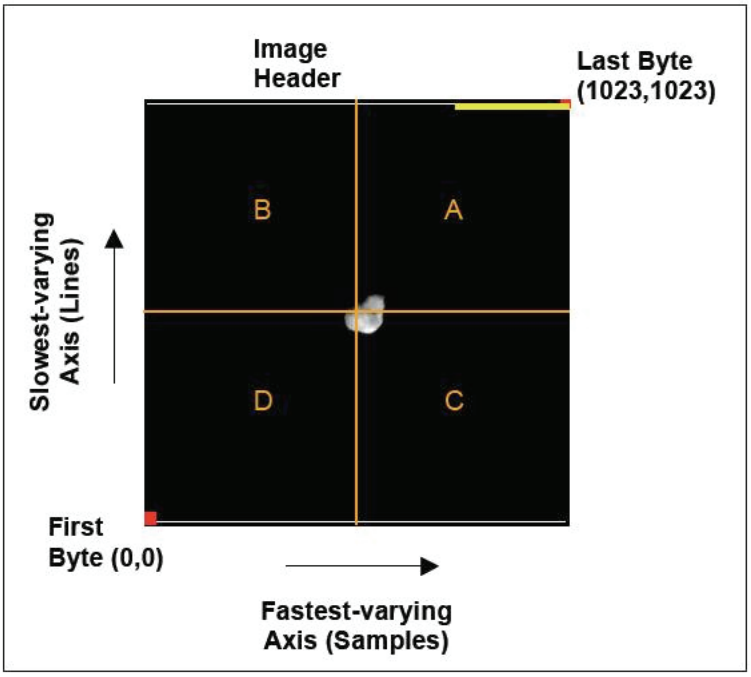

Figure 1. MRI image orientation and display conventions.

Although Figure 1 shows a full 1024x1024 MRI frame, the images we use in our analysis were taken with smaller image modes: 512x512, 256x256, and 128x128 pixels centered on the middle of the CCD. MRI data are unbinned (i.e., never binned).

As previously noted, the calibration pipeline corrects for the 1/6 decrease of signal in each of the two narrower central rows by the flat-field division so that the pixels in those two rows have the correct scene radiance in the calibrated RADREV images.

4.1.2 Centroid Coordinates

The second input to our photometric process is a list of centroid coordinates for the RADREV images. The opto-center of the coma was typically computed using the CNTRD routine found in the IDL Astronomy User's Library maintained by NASA Goddard Space Flight Center. These centers are good to approximately 1/3 pixel, given the under-sampled PSF. For images where the CNTRD routine did not converge because of trailing or other distortion, the centroid was selected manually to represent the apparent center of the coma. These centers are good to about a pixel, and can be identified by the fact that they are given to the nearest integer. The centroid coordinates, which are captured in the resulting photometry and error tables, are zero based with (0,0) assigned to center of the pixel in the lower-right corner an image.

4.2 Image Quality Flags

Before performing photometry, we manually inspect each RADREV image that has centroid coordinates and assign an image quality flag:

0: Good quality image
1: Star located within a 9-pixel radius of the centroid, possibly affecting small-aperture photometry
2: Cosmic ray located within a 9-pixel radius of the centroid, affecting small-aperture photometry
3: Context image for IR spectra
4: Saturated image (all with the nucleus fully resolved, during flyby)
5: Smeared image (spacecraft was in motion)
6: Corrupt image

We include only images with a quality flag of 0, 1, or 2 in our photometry process, which restricts our work to 30,136 frames. We call these images "good".

4.3 Cosmic Ray Removal

All MRI images have cosmic rays, with the number increasing with exposure time. To exclude cosmic rays from our photometric measurements, we process all "good" RADREV images through an IDL routine called IMGCLEAN that identifies very bright pixels and replaces those pixels with values derived by interpolation of the surrounding, well-behaved pixels. (IMGCLEAN performs a PSF match to avoid confusing cosmic rays with stars.) The cleaned RADREV images are then input to the CCD gap correction and photometry steps.

4.4 Gap Correction

Disk-integrated photometric measurements using aperture photometry that include the central two rows of RADREV images will be slightly distorted unless special adjustments are made. For our analysis, we correct for the central "gap" by resampling both halves of a RADREV image with linear interpolation to effectively push them inward, such that the

central two rows are reduced by a total width of 1/3 pixel. The procedure we implement starts the correction from the two central rows by decreasing their fluxes by 1/6 to undo the "scene radiance correction" of the flat field division performed by the calibration pipeline. Then our procedure moves 1/6 of the fluxes from the next adjacent rows outward for all rows. The first and last rows of the gap-corrected images contain lower fluxes than the real fluxes and should not be trusted. The resulting images have both aperture photometry and geometric distortion corrected. We apply this correction to all images before photometric measurements. The centroid of the comet is adjusted by 1/6 pixel inward if outside of the two central rows or recomputed in the corrected images using the procedure described in Section 4.1.2 if inside the two central rows. In theory, this correction does not change the photometry when the aperture size is smaller than the vertical distance between the comet centroid and the CCD center row. But because linear interpolation is involved with the non-linear brightness distribution of the coma, especially at small cometocentric distances, the photometry for small apertures that do not cross the two central rows is still slightly affected by the correction. See Section 4.7 for more details on the photometric uncertainties.

We find this method of gap correction significantly improves the photometry, most notably for measurements using the smallest apertures. In Figure 2, we see the lightcurve using a 2-pixel aperture is less noisy and shows a trend that is better aligned from point to point.

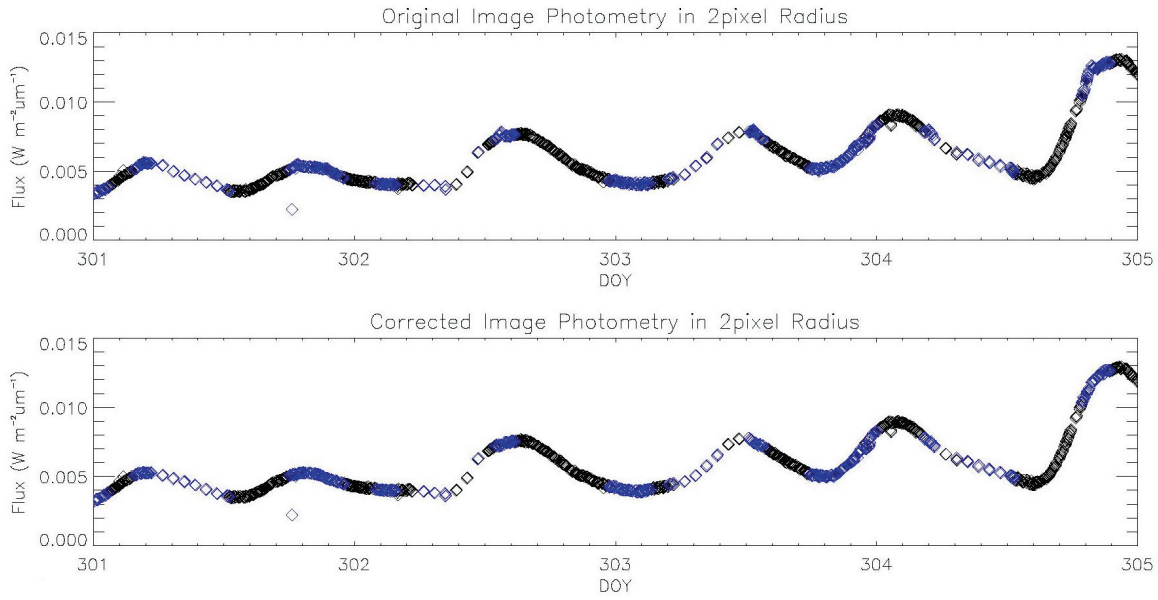

Figure 2. Aperture photometry for a 2-pixel radius using an original RADREV image (upper panel) and a gap-corrected image (lower panel).

4.5 Simple Aperture Photometry

We use the APER routine found in the IDL Astronomy User's Library to calculate photometry on the cleaned, calibrated RADREV images. No background was subtracted ("Skylevel=0"), and let the program compute the photometric errors of Poisson photon

counting noise using a CCD gain of 28.5 electrons/DN (Klaasen, et al., 2008). We use apertures from 1 to 30 pixels in radius with 1-pixel increments. We do not correct the resulting photometry and errors for phase angle or distance effects (i.e., the range between the spacecraft and the comet and the heliocentric distance of the comet). We output save the photometry measurements as flat ASCII tables by filter, with one row per image. We use an identical format for storing the error values.

We note that comet Hartley 2 was in a dense star-field as observed from the spacecraft during both approach and departure. The presence of many stars severely interferes with photometric measurements with large aperture sizes, such as >20 pixels in radius. We did not perform any rejection of stars in the simple aperture photometry measurements, but only flagged those images with stars located within 9 pixels from the comet. Therefore, researchers should exercise extreme caution when using the aperture photometry for radii larger than 9 pixels (up to where we checked for stars, images are flagged). For aperture radii > 20 pixels, we recommend using the photometric measurements from the technique described in Section 4.6.

4.6 Azimuthal Averaged Photometry

In order to minimize the contamination from background, we developed the so-called "azimuthal averaged photometry" procedure, which measures the integrated flux through the average radial profile of the comet with a resistant mean to filter out stars.

Specifically, we re-project an image into polar projection centered at the comet centroid, with 1-pixel incremental along the radial direction and 1-degree incremental along the azimuthal direction. Then using the RESISTANT_MEAN routine from IDL Astronomy User's Library, we take a 'resistant mean' along the azimuthal direction with a pre-set rejection threshold. This resistant-mean step rejects all bright pixels that belong to stars that are brighter than the threshold from the mean of the cometary coma. The mean represents an azimuthal average of the coma at a certain radial distance from the opto-center. The result of this step is an average radial profile of the coma. The total flux within a certain aperture is integrated along the average radial profile from the center to the aperture radius. The coma of Hartley 2 shows obvious azimuthal variations; the results of this method account for those variations.

The star rejection threshold for the resistant mean is set to be 3-sigma except for images taken through Clear1 and Green Continuum filters, for which a 3.5-sigma threshold is used. The reason for slightly higher threshold for those two filters is that the dust coma as observed through Clear1 and Green Continuum filters appears to have substantial azimuthal variations. A 3-sigma threshold would reject a small fraction of the coma in the azimuthal directions where coma is the brightest. The gas comae as observed through the CN and OH filters appear to be almost azimuthally symmetric.

The resistant mean step requires a sufficient fraction of pixels within the coma in order to reliably reject bright pixels of stars. Therefore, this procedure works better to filter out stars at larger radial distances from the center and is more reliable for the photometric measurements at relatively large aperture sizes. For this reason, as a general guideline,

we recommend researchers to use the aperture photometry described in Section 4.5 for aperture sizes smaller than 20-pixel radius, and the photometry results described in this section for larger aperture sizes. Occasionally, a bright star can be within just a few pixels from the center, rendering the calculation of resistant mean unreliable due to the small fraction of pixels in the coma at small radial distances. We flag all images with stars located within 9-pixels from the comet.

For the azimuthal averaged method we use the following 33 aperture radii, in pixels: 1, 2, 3, 4, 5, 6, 7, 8, 9, 10, 12, 14, 16, 18, 20, 25, 30, 35, 40, 45, 50, 55, 60, 80, 100, 120, 140, 160, 180, 200, 220, 240, 248. We do not correct the resulting photometry and errors for phase angle or distance effects (i.e., the range between the spacecraft and the comet and the heliocentric distance of the comet). We save the photometry measurements as flat ASCII tables by filter, with one row per image. We use an identical format for storing the error values.

4.7 Photometric Uncertainties

The sources of photometric uncertainties include absolute photometric calibration error, photon counting error, 1/3-pixel gap correction error, and other errors introduced during the processing for radial profile photometry. They have different characteristics and dominate over ranges of aperture sizes and images. We discuss them one by one below.

The absolute calibration error given for the MRI instrument is 20% for UV filters and 10% for all other filters (Klaasen, et al., 2013; Klaasen, et al., 2008). This calibration uncertainty is systematic, and is the same for all photometric data points. Since the photometric calibration of MRI is stable during the encounter (Klaasen, et al., 2013), this uncertainty affects all photometric data point by the same amount. It does not affect point-to-point variations.

The rejection of cosmic rays introduces uncertainty in the pixels affected by cosmic rays. The number of affected pixels is usually <1% of total pixels within the aperture, and the associated uncertainty is therefore much less than 1%, and negligible. We did not quantify this uncertainty in our analysis.

The photon counting noise follows Poisson statistics as the square root of total electrons accumulated in a pixel on the CCD. We calculated the photon counting noise with an MRI gain setting as 28.5 (Klaasen, et al., 2008). For Clear1 images, the photon counting noise is usually 1-1.5% for early approach images (E-60d to E-40d) with long exposures (60 s exposure time), and 1.5-3% for short exposures (20 s). Within E±40d, the uncertainties are typically <1% for long exposure images and <1.5% for short exposures. A few days from the closest encounter the uncertainties are typically <0.3%. For CN images, the photon counting noise is typically 1-3% for 1-pixel aperture photometry, and <1% for apertures >5 pixels. The uncertainties for OH photometry are similar to those for CN photometry.

The correction for the 1/3-pixel gap introduces uncertainties from the interpolation between pixels and the consequent loss of spatial resolution. We designated this

uncertainty as the difference of fluxes between corrected images and uncorrected images. As discussed earlier, for small apertures that do not cross the two central rows, the uncertainty calculated with this method is not exactly zero, but have some low absolute uncertainty values compared to larger apertures that cross the central rows. Once the aperture crosses the two central rows, the absolute uncertainty grows with aperture size, but the relative uncertainty reaches a maximum at aperture size of ~10 pixels larger than the distance between the centroid and the center row, then decrease. The typical uncertainty for gap correction is about ~2% with a long tail up to >10% for 1-pixel aperture, 0.5% for 10-pixel aperture with most <2%, and <1% for most images with aperture sizes >20 pixels. This estimate is the most conservative estimate and an upper limit of the actual uncertainty.

The above sources of uncertainties dominate the photometric measurements using simple aperture photometry method. The complicated processing for the azimuthal averaged photometry method introduces several more sources of uncertainties.

The dominant error sources for the azimuthal averaged profile photometry are the rejection of the large number of stars in the field and the assumption of radial symmetry. Unfortunately, both are hard to quantify. The azimuthal average of the coma at each radial distance effectively uses the resistant mean for filling the pixels that are rejected as affected by stars. Therefore, it is reasonable to assume that for those rejected pixels, their maximum possible value would be the maximum value of un-rejected pixels along the corresponding azimuthal profile, which is the threshold. The relative uncertainty is then estimated as the product of the resistant mean threshold and the fraction of rejected pixels in total number of pixels along the corresponding azimuthal profile.

The conversion of original image to polar coordinate involves bilinear interpolation. The accuracy of the interpolation depends on the flatness of the scene. With a radial profile close to a $1/\rho$ fall off, where ρ is the radial distance to the nucleus, the radial variation of the coma of Hartley 2 is large at smaller radial distances, and very small at large distances. Therefore, the relative uncertainty introduced by the interpolation only dominates small radial distances, and decreases with aperture size. Quantitative analysis shows that for aperture sizes >20 pixels, this uncertainty is negligible. The uncertainty grows as more and more stars are rejected in larger and larger apertures. Typically, this uncertainty is about a few percent, but could be up to 10% or even higher in occasional cases. For 20-pixel apertures, most photometry has uncertainties of 1%, and a small fraction of measurements have uncertainties of up to 10%. For 200-pixel apertures, most photometry has uncertainties of 0.5-3%.

The overall uncertainties of the photometric data are the combination of all relevant components in quadrature, assuming they are all independent of each other. Overall the point-to-point uncertainty is dominated by artifact rejection including cosmic rays and field stars. The absolute photometric uncertainty is dominated by the calibration error.

5 Known Constraints

Our photometry methods do not include a sky background subtraction. However, we determined sky background values for the Clear1 and CN filters by looking at the brightness profiles of images with the largest observed radial coverage of about 145,000 km, and evaluating longer exposures taken in the full-frame CCD mode of 1024x1024 pixels. For Clear1 images we find an average background intensity of $1e10^{-7}$ W m^{-2} $micron^{-1}$ $steradian^{-1}$ and for CN images $1e10^{-4}$ W m^{-2} $micron^{-1}$ $steradian^{-1}$ (Bodewits, et al., 2013). We did not derive a value for C2 and OH images because the signal to noise is too low for reliable measurements.

6 References

Belton, M.J.S., K.J, Meech, Karen, S. Chesley, Y. Pittichova, B. Carcich, M. Drahus, A. Harris, S. Gillam, J. Veverka, N. Mastrodemos, W. Owen, M.F. A'Hearn, S. Bagnulo, J. Bai, L. Barrera, F. Bastien, J.M. Bauer, J. Bedient, B.C. Bhatt, H. Boehnhardt, N. Brosch, M. Buie, P. Candia, W.-P. Chen, P. Chiang, Y-J. Choi, A. Cochran, C.J. Crockett, S. Duddy, T. Farnham, Y.R. Fernandez, P. Gutierrez, O.R. Hainaut, D. Hampton, K.A. Herrmann, H. Hsieh, M.A. Kadooka, H. Kaluna, J. Keane, M.-J.Kim, K. Klaasen, J. Kleyna, K. Krisciunas, L.M. Lara, T.R. Lauer, J.-Y. Li, J. Licandro, C.M. Lisse, S.C. Lowry, L. McFadden, N. Moskovitz, B. Mueller, D. Polishook, N.S. Raja, T. Riesen, D.K. Sahu, N. Samarasinha, G. Sarid, T. Sekiguchi, S. Sonnett, N.B. Suntzeff, B.W. Taylor, P. Thomas, G.P. Tozzi, R. Vasundhara, J.-B. Vincent, L.H. Wasserman, B. Webster-Schultz, B. Yang, T. Zenn, and H. Zhao, 2011, *'Stardust-NExT, Deep Impact, and the accelerating spin of 9P/Tempel 1'*, Icarus, Volume 213, Issue 1, p. 345-368, doi:10.1016/j.icarus.2011.01.006.

Bodewits, D., D. Hampton, K. Klaasen, S. Wissler, T. Farnham, and the DIXI team, *'Anomalous behavior of the MRI during approach to 103P/Hartley 2'*, EPOXI Mission Technical Report, 2011.

Bodewits, D., T.L. Farnham, M.S. Kelley, J.-Y. Li, J.L. Williams, K. Gonter, M.F. A'Hearn, M.J.S. Belton, S. Besse, L.M. Feaga, K.P. Klaasen, L. Kolokolova, K.J. Meech, C.M. Lisse, D.D Wellnitz, 2013, *'Gas and Dust in the Coma around Hartley 2'*, submitted to Icarus.

Hampton, D.L., J.W. Baer, M.A. Huisjen, C.C. Varner, A. Delamere, D.D. Wellnitz, M.F. A'Hearn, and K.P. Klaasen, 2005, An Overview of the Instrument Suite for the Deep Impact Mission, Space Science Reviews, 117, 43-93, doi:10.1007/s11214-005-3390-8.

Klaasen, K.P., M.F. A'Hearn, M. Baca, A. Delamere, M. Desnoyer, T. Farnham, O. Groussin, D. Hampton, S. Ipatov, J. Li, C. Lisse, N. Mastrodemos, S. McLaughlin, J. Sunshine, P. Thomas, and D. Wellnitz, 2008, Deep Impact Instrument Calibration, Rev. Sci. Instrum., 79, 091301, doi:10.1063/1.2972112.

Klaasen, K.P., S. Besse, D. Bodewits, B. Carcich, T. Farnham, L. Feaga, O. Groussin, D. Hampton, M. Huisjen, M.S. Kelley, S. McLaughlin, F. Merlin, S. Protopapa, J. Sunshine,

P. Thomas, and D. Wellnitz, 2013, *'EPOXI Instrument Calibration'*, Icarus, accepted for publication.

McLaughlin, S.A., B. Carcich, S.E. Sackett, and K.P. Klaasen, 2012, Epoxi 103P/HARTLEY2 Encounter - MRI Calibrated Images V1.0, NASA Planetary Data System, DIF-C-MRI-3/4-EPOXI-HARTLEY2-V1.0.